



Communication

An Electrically Tunable Terahertz Filter Based on Liquid-Crystal-Filled Slits with Wall Corrugations

Shi-Yang Zhang ^{1,2}, Jing Ma ³, Hai-Ling He ¹, Cheng-Guo Tong ², Huan Liu ¹, Ya-Xian Fan ^{1,2} 
and Zhi-Yong Tao ^{1,2,*} ¹ Guangxi Key Laboratory of Wireless Wideband Communication and Signal Processing, Guilin University of Electronic Technology, Guilin 541004, China² Academy of Marine Information Technology, Guilin University of Electronic Technology, Beihai 536000, China³ Shaanxi Key Laboratory for Theoretical Physics Frontiers, Institute of Modern Physics, Northwest University, Xi'an 710127, China

* Correspondence: zytao@guet.edu.cn

Abstract: We propose a type of hollow planar waveguide with corrugated walls, which can realize electrically tunable terahertz (THz) filtering by filling the slit with liquid crystals. When the THz signals propagate in a planar waveguide with periodic corrugations, the transmission spectrum always exhibits many pass and stop bands. Inserting a section of defects in the middle of the periodic corrugations can excite an extremely narrow transmission peak, which would be a very good THz filter for frequency division. To achieve tunability of this narrow linewidth THz filter, we also fill the slit between the two corrugated walls with a nematic liquid crystal. The effective refractive index of liquid crystals will change with the external electric field, thus tuning the frequency of the narrow peak. The simulated results show that the center frequency of the proposed filter can be tuned linearly in the frequency range of 0.984~1.023 THz by the external electric field. Moreover, the bandwidth of the filter can be adjusted from 3.2 GHz to 0.3 GHz by increasing the number of periods in the waveguide, and a maximum Q value of 2556 can be achieved when the number of periods at both sides of the defect is 12.

Keywords: periodic waveguides; narrow linewidth filter; electrical tuning

Citation: Zhang, S.-Y.; Ma, J.; He, H.-L.; Tong, C.-G.; Liu, H.; Fan, Y.-X.; Tao, Z.-Y. An Electrically Tunable Terahertz Filter Based on Liquid-Crystal-Filled Slits with Wall Corrugations. *Photonics* **2022**, *9*, 894. <https://doi.org/10.3390/photonics9120894>

Received: 1 November 2022

Accepted: 21 November 2022

Published: 23 November 2022

Publisher's Note: MDPI stays neutral with regard to jurisdictional claims in published maps and institutional affiliations.



Copyright: © 2022 by the authors. Licensee MDPI, Basel, Switzerland. This article is an open access article distributed under the terms and conditions of the Creative Commons Attribution (CC BY) license (<https://creativecommons.org/licenses/by/4.0/>).

1. Introduction

In recent years, terahertz (THz) technology has been applied in many fields, such as military [1], medical [2], communication [3], sensing [4], imaging [5], and security inspection [6]. The research on THz technology revolves around three main components, namely THz sources [7,8], detection [9], and its applications [10–12]. The THz application is closely related to the promotion of functional devices. The realization of high-power sources [13], absorbers [14,15], sensors [16], switches [17], and filters [18] has expanded the applications and aroused the interest of researchers. Constantly optimizing THz devices greatly benefits the development and promotion of THz technology, and many scholars are also committed to this research.

As a key device in the THz system, a THz filter can select a particular frequency band of signals to pass through or separate the frequency we need from a wideband, which greatly improves the working efficiency of the THz system [19–21]. Wilk et al. showed the first electron-switchable Bragg structure for THz frequencies [22]. The structure worked as a stop-band filter and a mirror. It has a 60 GHz-wide stop-band with a center frequency of 300 GHz, which can be removed by reorienting the liquid crystal molecules in an external electric field. Mendis et al. demonstrated a universal filter using a parallel plate waveguide, which provides low-pass, high-pass, band-pass, and band-stop filtering functions in the THz frequency range [23]. Vieweg et al. proposed a switchable THz notch filter [24]. The filter, comprising a liquid crystal layer, exhibited a half-wave retarder and an isotropic

layer in different states. Yan et al. demonstrated an optically controllable narrowband THz filter and a dual-wavelength filter using square lattice photonic crystals with defects [25]. Capmany et al. incorporated graphene into integrated coupled resonator waveguides to achieve reconfigurable operations [26]. Brunetti et al. proposed an ultra-high performance rejection filter based on a silicon double-loaded Mach Zehnder interferometer (MZI), which takes advantage of the high selectivity of the ring resonator and the large rejection ratio of MZI [27].

This paper proposes an electrically tunable THz filter based on liquid crystal (LC) filled slits with periodic wall corrugations. The wall corrugation with defects provides a narrow transmission peak filter while the tunability of the LC index is employed to tune the device. Section 2 presents the mechanism of defect mode generation in planar THz waveguides filled with liquid crystals. In Section 3, we discuss the effects of external electromagnetic fields on the filling LCs. Based on the experimental data, we simulate the effective refractive index of LCs with the varying electric field by a cubic polynomial model, which enables us to mimic the electrical tuning of the proposed THz filter. In Section 4, we will describe the various filter properties. Finally, a general conclusion is given.

2. Filter Structure

When a THz wave propagates through a waveguide with periodically corrugated walls, the Bragg resonance can be generated because the same modes in the waveguide interact with each other. The Bragg resonance can always result in the so-called Bragg gap in the spectrum, in which the THz radiation cannot pass through the waveguide. In our study, we truncate the periodic structure at its midpoint and insert a section of the straight waveguide, so the periodicity of the original waveguide is broken, but not its symmetry. This treatment allows THz waves to pass through the corrugated waveguide at specific frequencies in the previous Bragg gap, producing a narrow transmission peak. The transmission peak thus obtained is usually considered to be a defect mode.

The electrically tunable THz filter based on liquid-crystal-filled slits with corrugations proposed in this paper is shown in Figure 1. It is a planar waveguide with a periodically undulating structure etched on the inner wall of high-density polyethylene (HDPE). Then a thin film of gold with a thickness of 1 μm is coated on the upper and lower surfaces of the waveguide. The hollow part of the waveguide is filled with a nematic LC (E7) and then sealed with 10 μm -thick HDPE, which connects the four boundaries of the upper and the lower plates. In Figure 1, HDPE is only drawn at the inlet and outlet ports of the waveguide to facilitate the display of the structure. Gold is chosen to be coated on the inner wall of the waveguide because gold has low loss in the THz band and can serve as a perfect electrical conductor [28]. However, HDPE has high transmittance and low loss in the THz band, which can significantly reduce the loss before the THz wave enters the waveguide [29]. The waveguide inner-wall period undulation structure has a rectangular shape, the period $\lambda = 220 \mu\text{m}$, the undulation depth $a = 71.6 \mu\text{m}$, the average distance $d = 214 \mu\text{m}$, the inserted defect length is $w = 264 \mu\text{m}$, and the number of periods is 20. The length of the straight waveguide at the inlet and outlet of the waveguide $l = 275 \mu\text{m}$. The THz source produces a horn-shaped beam, with the signal incident from the left end of the waveguide and out from the right end. The THz radiation is guided in the layer of LCs between the two gold-coated plates, and the inset in Figure 1 depicts the cross-sectional view of the guided mode. The three-dimensional Euclidean space coordinate system is also shown in the left corner of Figure 1, in which the x -axis is along the horizontal symmetry axis of the waveguide. Due to the inner wall's gold-coated upper and lower surfaces, the THz waves will have Bragg resonance in the waveguide due to the periodic corrugations, thus creating a Bragg gap. The straight waveguide we introduce in the periodic structure can excite a defect mode with a very narrow linewidth.

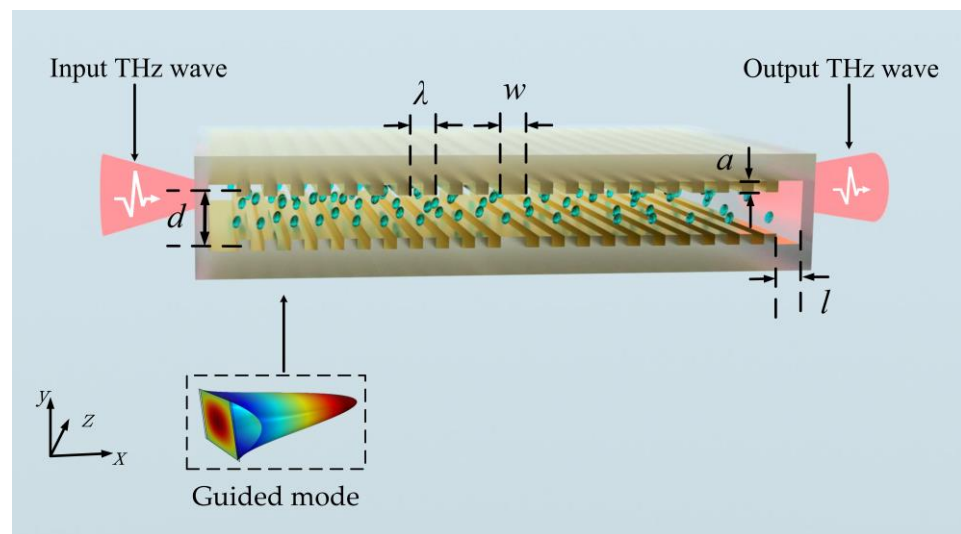


Figure 1. Structure of the proposed electrically tunable THz filter. A layer of gold is coated on the corrugated HDPE substrates to form the wall of waveguides. The big blue dots denote the filled LCs, and the THz radiation passes through the slit from left to right along *x*-axis. The inset depicts the cross-sectional view of the guided mode.

To actively modulate the operating frequency of this defect mode, we have introduced nematic LCs in the waveguide cavity [30]. Liquid crystals are widely used nonlinear dielectric materials because of their special physical, chemical, and optical properties [31–33]. In the present study, the nematic LCs (E7) are selected as the material to fill the waveguide slit because E7 has sensitive electrical tunability in the terahertz band and its loss is very small [34], which is ignored in the simulation.

LC (E7) molecules are very sensitive to the external electric field. As long as the external electric field changes slightly, the arrangement of LC (E7) molecules will change. When the voltage is turned off, that is $E = 0$ V/mm, LCs molecules are randomly arranged, and LC is an isotropic medium. When a bias voltage is applied to LCs, the dipoles will be arranged along the direction of the electric field, and the LC turns to an anisotropic medium, resulting in the changes of LC (E7) optical properties—that is, the effective refractive index n_{eff} will change with the varying external electric field. The phenomenon that the optical properties of LC change due to the external electric field has been called the photoelectric effect of LCs. Yang et al. have experimentally measured the refractive index n_{eff} of liquid crystals in the frequency range of 0.5 THz to 1.5 THz when the electric field E ranges from 0 V/mm to 7 V/mm [35]. Although our proposed structure is different, our design only depends on the change of effective refractive index n_{eff} brought by LC photoelectric effects, and its optical properties are similar. Since our filter works in the range of 0.7 THz~1.4 THz, we read the effective refractive index n_{eff} of the LCs in this frequency band from the experimental data. We employ the curve-fitting algorithm to process the data and obtain the cubic polynomial fitting of the effective refractive index n_{eff} of the LCs with a different electric field as follows:

$$n_{eff} = a \times f^3 + b \times f^2 + c \times f + d. \tag{1}$$

The optimal coefficients and R^2 are shown in Table 1. It can be seen that R^2 is close to 1, which means that the fitting results are in good agreement with the experimental data. Thus, we used this cubic polynomial fit in our simulations.

Table 1. Optimal coefficients for the cubic polynomial fit.

E (V/mm)	a	b	c	d	R^2
0	0.0656	−0.1801	0.1296	1.592	0.9993
3	0.0606	−0.1859	0.1615	1.596	0.9971
4	0.0246	−0.0600	0.0322	1.650	0.9919
5	0.0743	−0.2360	0.2328	1.595	0.9931
6	0.0578	−0.1914	0.1925	1.622	0.9955
7	0.0733	−0.2384	0.2410	1.619	0.9945

3. Electrical Tuning

Using the finite element method (FEM) of COMSOL Multiphysics, we calculated the transmission of the corrugated waveguides. In the simulation, we take the refractive index of HDPE as 1.5 [36], and the dielectric function of Au is given by the Drude model [37]. When the electric intensity is set to $E = 0$ V/mm, the blue dashed line in Figure 2 shows the transmission of the waveguide without the defect, and the solid red line denotes the transmission of the waveguide with the defect. As expected, there is a Bragg forbidden band in the purely periodic waveguide; the frequency range is 0.991~1.065 THz, as shown by the blue dashed line in Figure 2. After introducing defects, the Bragg forbidden band gets slightly wider than a purely periodic waveguide, with a frequency range of 0.986~1.065 THz. A narrow transmission peak appears near 1.039 THz, as shown by the solid red line in Figure 2. This anomalous transmission peak is extremely narrow, which is a good candidate for realizing THz narrowband filters. When the waveguide is enlarged or reduced, the transmission peak will move to the low or high frequencies, respectively, but the structure of the spectral band will not change. The size influence of waveguide structure on the spectral band has been discussed in detail by Ma et al. [38].

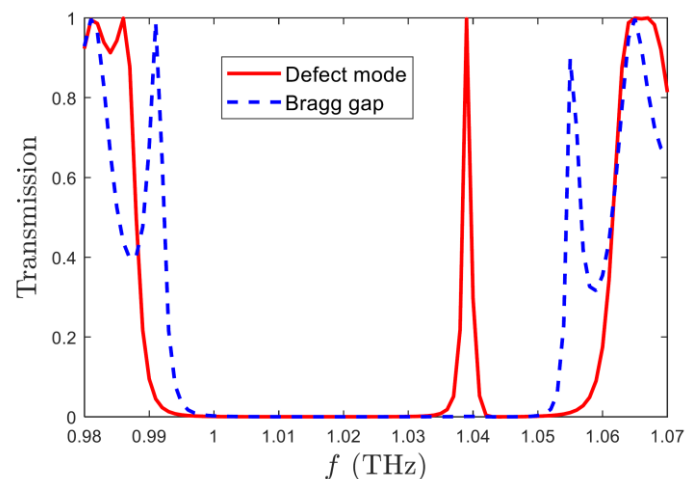


Figure 2. Spectra of planar THz waveguides with (the solid red line) and without (the blue dashed line) defects.

To further analyze the defect mode of the waveguide, we simulated the THz waves on the horizontal symmetry axis of the waveguide. Figure 3a represents the distribution of the electric field component E_z along the x -axis. Based on the simulated electric fields, we performed the Fourier transform to obtain the dispersion curve of the defect structure, as shown in Figure 3b. It can be seen from Figure 3 that the THz waves interact with the periodic structure, and there is a significant energy decay at the frequency corresponding to the Bragg gap in Figure 2, while the introduction of the defect structure creates a very narrow transmission with energy accumulation in this gap.

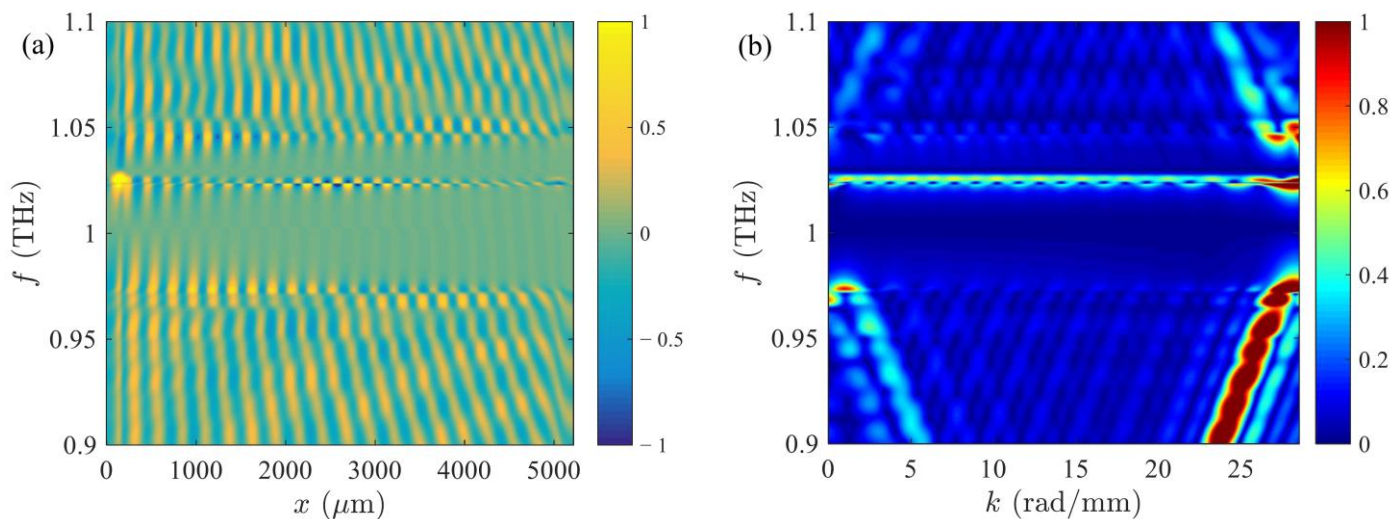


Figure 3. (a) Spectra along the x -axis for the waveguide with the defect; (b) dispersion curves depicting a defect mode between 1 THz and 1.05 THz.

4. Filter Performance

Electrical tunability is achieved when we fill the filter cavity with LCs. We numerically simulate the propagation of the THz waves in the Bragg defect structure with the FEM. We apply external electric fields of different intensities to the filter to obtain the operating band of narrow-band pulses, as shown in Figure 4a. When the electric field E rises from 3 V/mm to 7 V/mm, the narrow-band pulse moves from the high to the low-frequency range. The center frequency of the defect mode is 1.023 THz when the electric field is 3 V/mm, and it moves to 0.984 THz when the electric field increases to 7 V/mm. Here, we have achieved a series of transmission peaks when the bias voltage increases, while a similar experimental phenomenon has been observed by Deng et al. with a LC-based metasurface [15]. An absorption peak around 100 GHz moved from the high to the low frequency with a narrow band when the voltage increased to 10 V.

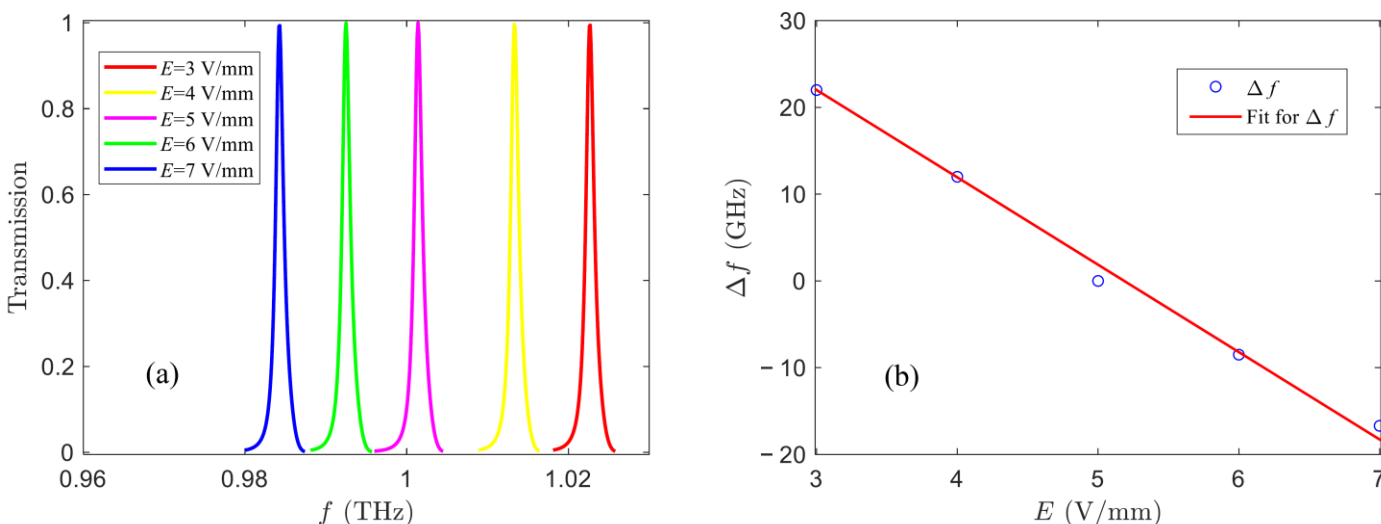


Figure 4. Electrically tuning of the narrow band THz filter. (a) Transmission peak shifting with the external electric field; (b) peak frequency shift of the filter and its best fit denoted by the blue circles and solid red line, respectively.

To investigate the sensitivity of the proposed narrowband filter to the external electric field, we read the center frequency of the peak at each electric field and fit it into a cubic

polynomial model of the electric field E , as shown in Figure 4b. The best-fitting curve for the frequency shift Δf from 1 THz is:

$$\Delta f = -9.79 \times E + 51.71. \tag{2}$$

R^2 of the linear fitting is 0.9946, indicating the excellent fitting effect. The fitting results show that the pulse peak is linearly shifted to lower frequencies as the field E increasing. A 1 V/mm increase of the external electric field results in a 9.79 GHz frequency shift of the filter. Thus, it is possible to make the filter operate in the frequency band as desired by adjusting the external electric field. In applications, the response time of the proposed filter is related to the LC molecule rotation speed when the external electric field changes. The response time of LCs to voltage has been experimentally measured, and the achieved recovery time is about several seconds [15].

In the study of periodically structured waveguides, the number of periods is an important parameter. Therefore, the number of periods is also discussed in our study. The waveguide has a total of 20 periods, that is, 10 periods at both ends after inserting the defect. n is the number of periods at both ends of the defect. We use the FEM to numerically simulate the waveguide structure with $n = 8\sim 12$ periods at both ends of the middle defect and obtain the transmission spectrum of the narrowband peaks, as shown in Figure 5. It can be seen from the figure that with the increasing number of waveguide periods, the peak value of the narrowband is almost the same, as well as the almost total transmission. The position of the peak value hardly moves, but the bandwidth narrows.

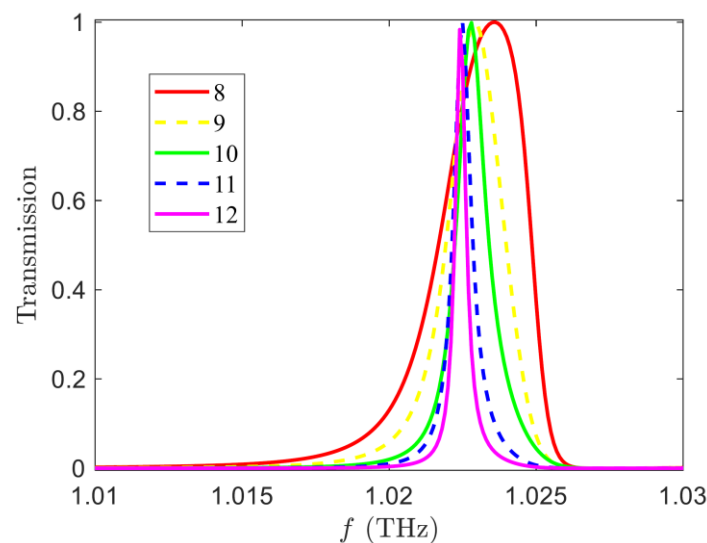


Figure 5. Transmission peaks of the filters with a different number of periods.

To further explore the effect of the variation in the number of periods on the filter performance, the bandwidth of the filter and the magnitude of the Q-factor have also been investigated. Here, the Q-factor is defined as the ratio of the peak frequency to its full width at half height, which is an important index of the filter performance. The larger the Q-factor, the better the filter performance. The obtained bandwidth and the variation trend of the Q-factor are shown in Figure 6. As the number of waveguide periods increases, the bandwidth of the peak decreases sharply, and the Q-factor increases gradually. It can be predicted that if we continue to increase the number of periods, it will result in a higher Q factor. However, the more periods, the larger the structure, which would limit applications. So, only the maximum $n = 12$ is considered in our simulation, and there will be a trade-off between the high Q factor and the large size device in applications. In our calculations, the bandwidth decreases from 3.2 GHz to 0.3 GHz, indicating that this filter structure has a narrowband filtering function with adjustable bandwidth. The filter reaches a maximum Q-factor of 2556 when the number of periods at both ends of the defect is 12.

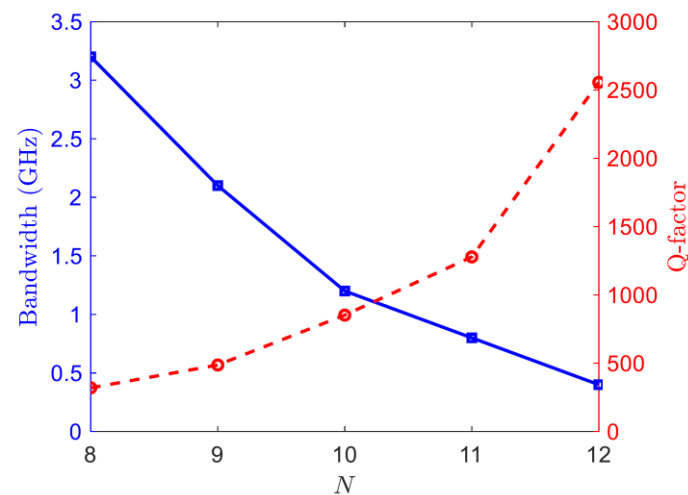


Figure 6. Filter bandwidth (the solid blue line) and the Q-factor (the dotted red line) for the filters with different periods.

5. Conclusions

We have proposed an electrically tunable THz filter based on the corrugated planar THz waveguide filled by LCs. The periodic corrugations create the Bragg gap in the frequency spectrum, while the inserted defect results in the narrow transmission peak, which can be employed in the THz filtering applications. The filled LCs can be affected by the external electric field, which can change the effective refractive index of LCs. Considering the experimentally measured index of LCs, we can realize an electrically tunable narrow-band THz filter by varying the external electric field. The proposed filter transmission is very close to 1, and the narrowest bandwidth reaches 0.3 GHz with a maximum Q-factor of 2556. Its center frequency tunable band range is 0.984~1.023 THz, which can also be changed by enlarging or reducing the structure size of the filter. Due to its impressive performance, this electrically tunable filter could find applications in various THz systems, especially for the frequency division multiplexing in further THz communication.

Author Contributions: Conceptualization, Y.-X.F. and Z.-Y.T.; methodology, S.-Y.Z. and J.M.; validation, J.M.; formal analysis, S.-Y.Z., J.M., C.-G.T. and H.L.; investigation, S.-Y.Z. and H.-L.H.; writing—original draft preparation, S.-Y.Z.; writing—review and editing, Y.-X.F. and Z.-Y.T.; visualization, S.-Y.Z.; supervision, Y.-X.F. and Z.-Y.T. All authors have read and agreed to the published version of the manuscript.

Funding: This research was supported by the Guangxi Natural Science Foundation (2020GXNSFBA15 9047, 2021GXNSFAA220073, 2021GXNSFAA220086, and 2021GXNSFDA075006), the National Natural Science Foundation of China (12064005 and 62001132), the Innovation Project of GUET Graduate Education (2022YCXS033 and 2022YCXS041), and the Double First-Class University Construction Project of Northwest University.

Institutional Review Board Statement: Not applicable.

Informed Consent Statement: Not applicable.

Data Availability Statement: The data presented in this study are available on request from the corresponding author.

Conflicts of Interest: The authors declare no conflict of interest.

References

- Huang, Y.-W.; Tseng, T.-F.; Kuo, C.-C.; Hwang, Y.-J.; Sun, C.-K. Fiber-Based Swept-Source Terahertz Radar. *Opt. Lett.* **2010**, *35*, 1344–1346. [[CrossRef](#)] [[PubMed](#)]
- Siegel, P.H. Terahertz Technology in Biology and Medicine. *IEEE Trans. Microw. Theory Tech.* **2004**, *52*, 2438–2447. [[CrossRef](#)]

3. Ibraheem, I.A.; Krumbholz, N.; Mittleman, D.; Koch, M. Low-Dispersive Dielectric Mirrors for Future Wireless Terahertz Communication Systems. *IEEE Microw. Wirel. Compon. Lett.* **2008**, *18*, 67–69. [[CrossRef](#)]
4. Cunningham, J.; Wood, C.; Davies, A.G.; Tiang, C.K.; Tosch, P.; Evans, D.A.; Linfield, E.H.; Hunter, I.C.; Missous, M. Multiple-Frequency Terahertz Pulsed Sensing of Dielectric Films. *Appl. Phys. Lett.* **2006**, *88*, 071112. [[CrossRef](#)]
5. Qiu, F.; Tan, Z.; Fu, Z.; Wan, W.; Li, M.; Wang, C.; Cao, J. Reflective Scanning Imaging Based on a Fast Terahertz Photodetector. *Opt. Commun.* **2018**, *427*, 170–174. [[CrossRef](#)]
6. Knipper, R.; Brahm, A.; Heinz, E.; May, T.; Notni, G.; Meyer, H.-G.; Tunnermann, A.; Popp, J. THz Absorption in Fabric and Its Impact on Body Scanning for Security Application. *IEEE Trans. Terahertz Sci. Technol.* **2015**, *5*, 999–1004. [[CrossRef](#)]
7. Biedron, S.G.; Lewellen, J.W.; Milton, S.V.; Gopalsami, N.; Schneider, J.F.; Skubal, L.; Li, Y.; Virgo, M.; Gallerano, G.P.; Doria, A.; et al. Compact, High-Power Electron Beam Based Terahertz Sources. *Proc. IEEE* **2007**, *95*, 1666–1678. [[CrossRef](#)]
8. Mitryukovskiy, S.I.; Liu, Y.; Prade, B.; Houard, A.; Mysyrowicz, A. Effect of an External Electric Field on the Coherent Terahertz Emission from Multiple Filaments in Air. *Appl. Phys. B* **2014**, *117*, 265–269. [[CrossRef](#)]
9. Saeedkia, D.; Safavi-Naeini, S. Terahertz Photonics: Optoelectronic Techniques for Generation and Detection of Terahertz Waves. *J. Light. Technol.* **2008**, *26*, 2409–2423. [[CrossRef](#)]
10. Jackson, J.B.; Bowen, J.; Walker, G.; Labaune, J.; Mourou, G.; Menu, M.; Fukunaga, K. A Survey of Terahertz Applications in Cultural Heritage Conservation Science. *IEEE Trans. Terahertz Sci. Technol.* **2011**, *1*, 220–231. [[CrossRef](#)]
11. Zouaghi, W.; Thomson, M.D.; Rabia, K.; Hahn, R.; Blank, V.; Roskos, H.G. Broadband Terahertz Spectroscopy: Principles, Fundamental Research and Potential for Industrial Applications. *Eur. J. Phys.* **2013**, *34*, S179–S199. [[CrossRef](#)]
12. Watanabe, S. Terahertz Polarization Imaging and Its Applications. *Photonics* **2018**, *5*, 58. [[CrossRef](#)]
13. Yardimci, N.T.; Cakmakyapan, S.; Hemmati, S.; Jarrahi, M. A High-Power Broadband Terahertz Source Enabled by Three-Dimensional Light Confinement in a Plasmonic Nanocavity. *Sci. Rep.* **2017**, *7*, 4166. [[CrossRef](#)]
14. Kong, H.; Li, G.; Jin, Z.; Ma, G.; Zhang, Z.; Zhang, C. Polarization-Independent Metamaterial Absorber for Terahertz Frequency. *J. Infrared Millim. Terahertz Waves* **2012**, *33*, 649–656. [[CrossRef](#)]
15. Deng, G.; Hu, H.; Mo, H.; Yin, Z.; Lu, H.; Hu, M.; Li, J.; Yang, J. Liquid Crystal-Based Wide-Angle Metasurface Absorber with Large Frequency Tunability and Low Voltage. *Opt. Express* **2022**, *30*, 22550–22561. [[CrossRef](#)] [[PubMed](#)]
16. Xu, L.-L.; Gong, Y.; Fan, Y.-X.; Tao, Z.-Y. A High-Resolution Terahertz Electric Field Sensor Using a Corrugated Liquid Crystal Waveguide. *Crystals* **2019**, *9*, 302. [[CrossRef](#)]
17. Choi, S.B.; Park, D.J. Ultrafast Optical Switching of Terahertz Wave Transmission through Semiconductor/Metallic Subwavelength Slot Antenna Hybrid Structure. *Curr. Appl. Phys.* **2016**, *16*, 109–114. [[CrossRef](#)]
18. Li, J. Fast-Tunable Terahertz Wave Filter Based on Kerr Medium. *Opt. Laser Technol.* **2014**, *56*, 263–268. [[CrossRef](#)]
19. Busch, S.F.; Schumann, S.; Jansen, C.; Scheller, M.; Koch, M.; Fischer, B.M. Optically Gated Tunable Terahertz Filters. *Appl. Phys. Lett.* **2012**, *100*, 261109. [[CrossRef](#)]
20. Rui, F.; Li, W. A Zone Plate as a Tunable Terahertz Filter. *Chin. Phys. Lett.* **2010**, *27*, 064201. [[CrossRef](#)]
21. Li, S.; Liu, H.; Sun, Q.; Huang, N. A Tunable Terahertz Photonic Crystal Narrow-Band Filter. *IEEE Photon. Technol. Lett.* **2015**, *27*, 752–754. [[CrossRef](#)]
22. Wilk, R.; Vieweg, N.; Kopschinski, O.; Koch, M. Liquid Crystal Based Electrically Switchable Bragg Structure for THz Waves. *Opt. Express* **2009**, *17*, 7377–7382. [[CrossRef](#)] [[PubMed](#)]
23. Mendis, R.; Nag, A.; Chen, F.; Mittleman, D.M. A Tunable Universal Terahertz Filter Using Artificial Dielectrics Based on Parallel-Plate Waveguides. *Appl. Phys. Lett.* **2010**, *97*, 131106. [[CrossRef](#)]
24. Vieweg, N.; Born, N.; Al-Naib, I.; Koch, M. Electrically Tunable Terahertz Notch Filters. *J. Infrared Millim. Terahertz Waves* **2012**, *33*, 327–332. [[CrossRef](#)]
25. Yan, D.; Li, J.; Jin, L. Light-Controlled Tunable Terahertz Filters Based on Photoresponsive Liquid Crystals. *Laser Phys.* **2019**, *29*, 025401. [[CrossRef](#)]
26. Capmany, J.; Domenech, D.; Munoz, P. Silicon Graphene Reconfigurable CROWS and SCISSORS. *IEEE Photon. J.* **2015**, *7*, 2700609. [[CrossRef](#)]
27. Brunetti, G.; Sasanelli, N.; Armenise, M.N.; Ciminelli, C. High Performance and Tunable Optical Pump-Rejection Filter for Quantum Photonic Systems. *Opt. Laser Technol.* **2021**, *139*, 106978. [[CrossRef](#)]
28. Azad, A.K.; Zhang, W. Resonant Terahertz Transmission in Subwavelength Metallic Hole Arrays of Sub-Skin-Depth Thickness. *Opt. Lett.* **2005**, *30*, 2945–2947. [[CrossRef](#)]
29. Chen, X.L.; Chen, X.; Li, D.S.; Zhu, Z.Y. Dielectric Properties of Carbon-Materials-Filled Composites Characterized by Terahertz Time-Domain Spectroscopy. *Adv. Mater. Res.* **2011**, *295–297*, 1408–1413. [[CrossRef](#)]
30. Park, H.; Parrott, E.P.J.; Fan, F.; Lim, M.; Han, H.; Chigrinov, V.G.; Pickwell-MacPherson, E. Evaluating Liquid Crystal Properties for Use in Terahertz Devices. *Opt. Express* **2012**, *20*, 11899–11905. [[CrossRef](#)] [[PubMed](#)]
31. Zhang, L.; Fan, Y.-X.; Liu, H.; Xu, L.-L.; Xue, J.-L.; Tao, Z.-Y. Hypersensitive and Tunable Terahertz Wave Switch Based on Non-Bragg Structures Filled with Liquid Crystals. *J. Light. Technol.* **2017**, *35*, 3092–3098. [[CrossRef](#)]
32. Wu, H.Y.; Hsieh, C.F.; Tang, T.T.; Pan, R.P.; Pan, C.L. Electrically Tunable Room-Temperature $2/\text{Spl Pi}$ Liquid Crystal Terahertz Phase Shifter. *IEEE Photon. Technol. Lett.* **2006**, *18*, 1488–1490.
33. Ge, S.-J.; Shen, Z.-X.; Chen, P.; Liang, X.; Wang, X.-K.; Hu, W.; Zhang, Y.; Lu, Y.-Q. Generating, Separating and Polarizing Terahertz Vortex Beams via Liquid Crystals with Gradient-Rotation Directors. *Cryst.* **2017**, *7*, 314. [[CrossRef](#)]

34. Li, X.; Tan, N.; Pivnenko, M.; Sibik, J.; Zeitler, J.A.; Chu, D. High-Birefringence Nematic Liquid Crystal for Broadband THz Applications. *Liq. Cryst.* **2016**, *43*, 955–962. [[CrossRef](#)]
35. Yang, L.; Fan, F.; Chen, M.; Zhang, X.; Chang, S.-J. Active Terahertz Metamaterials Based on Liquid-Crystal Induced Transparency and Absorption. *Opt. Commun.* **2017**, *382*, 42–48. [[CrossRef](#)]
36. Chen, X.; Ma, M.; Yang, X.; Yang, K.; Liu, D.; Te, J.; Wu, S.; Zhu, Z. Optical Properties of Carbon Materials Filled HDPE Composites in THz Region. *Nucl. Sci. Tech.* **2009**, 265–270.
37. Ordal, M.A.; Long, L.L.; Bell, R.J.; Bell, S.E.; Bell, R.R.; Alexander, R.W.; Ward, C.A. Optical Properties of the Metals Al, Co, Cu, Au, Fe, Pb, Ni, Pd, Pt, Ag, Ti, and W in the Infrared and Far Infrared. *Appl. Opt.* **1983**, *22*, 1099–1120. [[CrossRef](#)] [[PubMed](#)]
38. Ma, J.; Liu, H.; Zhang, S.-Y.; Zou, W.-L.; Fan, Y.-X.; Tao, Z.-Y. Terahertz Resonances of Transverse Standing Waves in a Corrugated Plate Waveguide. *IEEE Photon. J.* **2022**, *14*, 5929508. [[CrossRef](#)]